Mon. Not. R. Astron. Soc. **353,** 1107–1116 (2004) doi:10.1111/j.1365-2966.2004.08132.x

Night sky brightness at sites from DMSP-OLS satellite measurements

P. Cinzano[1,2]★ and C. D. Elvidge[3]

[1]*Dipartimento di Astronomia, Università di Padova, Vicolo dell'Osservatorio 2, I-35122 Padova, Italy*
[2]*Istituto di Scienza e Tecnologia dell'Inquinamento Luminoso (ISTIL), Via Roma 13, I-36016 Thiene, Italy*
[3]*NOAA National Geophysical Data Center, 325 Broadway, Boulder, CO 80303, USA*

Accepted 2004 June 17. Received 2004 May 26; in original form 2004 April 20

ABSTRACT

We apply the sky brightness modelling technique introduced and developed by Roy Garstang to high-resolution satellite measurements of upward artificial light flux carried out with the US Air Force Defense Meteorological Satellite Program Operational Linescan System and to GTOPO30 (a global digital elevation model by the US Geological Survey's EROS Data Centre) digital elevation data in order to predict the brightness distribution of the night sky at a given site in the primary astronomical photometric bands for a range of atmospheric aerosol contents. This method, based on global data and accounting for elevation, Earth curvature and mountain screening, allows the evaluation of sky glow conditions over the entire sky for any site in the world, to evaluate its evolution, to disentangle the contribution of individual sources in the surrounding territory and to identify the main contributing sources. Sky brightness, naked eye stellar visibility and telescope limiting magnitude are produced as three-dimensional arrays, the axes of which are the position on the sky and the atmospheric clarity. We compare our results with available measurements.

Key words: scattering – atmospheric effects – light pollution – site testing.

1 INTRODUCTION

The change in the light in the night environment due to the introduction of artificial light is true pollution, a growing adverse impact on the night. Pollution means 'impairment or alteration of the purity of the environment' or of its chemical/physical parameters. This alteration of natural light at night, called light pollution, can and does impact the environment and the health of the beings living in it (animals, plants and man), as shown by hundreds of scientific studies and reports (see, for example, Cinzano 1994; Erren & Piekarski 2002; Rich & Longcore 2002). The growth of night sky brightness is one of the many effects of artificial light being wasted in the environment. It is a serious problem. It endangers not only astronomical observations but also the perception of the Universe around us (see Crawford 1991; Kovalewski 1992; McNally 1994; Isobe & Hirayama 1998; Cinzano 2000a, 2002; Cohen & Sullivan 2001; Schwarz 2003 and the International Dark-Sky Association Web site, www.darksky.org). The starry sky constitutes mankind 's only window to the universe beyond the Earth. A fundamental heritage for the culture, both humanistic and scientific, and an important part of the our night-time landscape patrimony is going to be lost, both for those alive today and for our children and their children. The growing worldwide concern about light pollution and its effects requires methods for monitoring this situation.

★E-mail: cinzano@pd.astro.it

The modelling of the brightness distribution of the night sky at a given site is important for evaluating its suitability for astronomical observations, to quantify its sky glow, and to recognize endangered parts of the sky hemisphere. Night sky models are useful for studying the relationship of sky glow to atmospheric conditions and for evaluating future changes in sky glow. Modelling is also required in order to disentangle the contribution of sources, such as individual cities, in order to recognize those areas producing the strongest impact and to undertake action to limit light pollution.

In 1986 Roy Garstang introduced a modelling technique, developed and refined in the subsequent years (Garstang 1986, 1987, 1988, 1989a,b, 1991a,b,c, 1992, 1993, 2000a), to compute light pollution propagation in the atmosphere. He estimated the night sky brightness at many sites based on geographical position, altitude and population of polluting cities. Cinzano (2000b) used Garstang's models to disentangle the impact of individual cities, constraining free functions with the condition that the sum of all the contributions to natural sky brightness fit the observed sky brightness. However, up-to-date population data are not easily available worldwide, and upward light emission is not strictly proportional to population. Some polluting sources, such as industrial areas and airports, have very low population density but very high light emission. The US Air Force Defense Meteorological Satellite Program (DMSP) Operational Linescan System (OLS) acquires direct observations of nocturnal lighting, making it possible to map the spatial distribution of night-time lights (Sullivan 1989, 1991; Elvidge et al. 1997a,b,c, 2001, 2003a,b; Gallo et al. 2003; Henderson et al. 2003). Most

night-time OLS observations of urban centres are saturated, making the data of limited value for modelling purposes. However, Elvidge et al. (1999) were able to produce a radiance calibrated global night-time lights product, using OLS data acquired at reduced gain settings, suitable for the quantitative measurement of upward light emission (e.g. Isobe & Hamamura 2000; Luginbuhl 2001; Osman et al. 2001) and the evaluation of the artificial sky brightness produced by it (e.g. Falchi 1998; Falchi & Cinzano 2000).

Cinzano et al. (2000) presented a method of mapping the artificial sky brightness across large territories in a given direction of the sky by evaluating the upward light emission from DMSP high-resolution radiance-calibrated data (Elvidge et al. 1999) and the propagation of light pollution using Garstang's models. A world atlas of the artificial night sky brightness at sea level was obtained in this way (Cinzano, Falchi & Elvidge 2001b). This method was extended by Cinzano, Falchi & Elvidge (2001a) to the mapping of naked eye and telescopic limiting magnitude based on the Schaefer (1990) and Garstang (2000b) approach and the GTOPO30 elevation data. We extend and apply their method to the computation of the distribution of the night sky brightness and the limiting magnitude over the entire sky at any site for a range of atmospheric conditions and accounting for mountain screening. In Section 2 we describe the computation of three-dimensional arrays, whose axes are the position on the sky and the atmospheric clarity, and present our improvements. In Section 3 we describe input data. In Section 4 we deal with the disentangling of individual sources. In Section 5 we discuss the application and in Section 6 we present comparisons with available measurements. Conclusions are given in Section 7.

2 COMPUTATION OF THE HYPERMAPS

Artificial and natural sky brightness vary depending on the aerosol content of the atmosphere. The stellar extinction also varies substantially depending on the aerosol content of the local atmosphere. This in turn affects the limiting magnitude. So any map of the sky of a site is a function of the aerosol content for which it has been computed.

We refer to a hypermap as a set of maps of the night sky brightness for a range of aerosol contents, $b(z, \omega, K)$, where z is the zenith distance, ω is the azimuth and K is the aerosol content expressed by the atmospheric clarity (Garstang 1986, 1989a). As Fig. 1 shows, values on planes of the space of the variables perpendicular to the K-axis give maps of the sky brightness for the given atmospheric clarity, values along a line parallel to the K-axis give the brightness in the given point of the sky when the atmospheric aerosol content

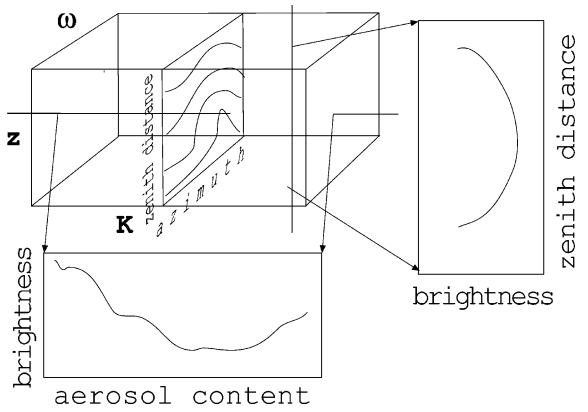

Figure 1. Projections of the hypermap on different planes.

changes, values along lines perpendicular to the K- and ω-axis give the sky brightness along an almucantar for the given atmospheric clarity.

At a site in (x', y') the hypermap is given by

$$b(z, \omega, K) = \int_{-\infty}^{+\infty} \int_{-\infty}^{+\infty} e(x, y) f(x, y, x', y', z, \omega, K)\, \mathrm{d}x\, \mathrm{d}y, \tag{1}$$

where $f(x, y, x', y', z, \omega, K)$ is the light pollution propagation function, i.e. the artificial sky brightness at (x', y') in the direction given by (z, ω) per unit of upward light emission $e(x, y)$ produced by the unitary area in (x, y) when atmospheric aerosol content is K. If we divide a territory into land areas (h, l) with position (x_h, y_l), the hypermap can be expressed as a tridimensional array $b_{i,j,k}$ given by

$$b_{i,j,k} = \sum_h \sum_l e_{h,l} f(x_h, y_l, x', y', z_i, \omega_j, K_k), \tag{2}$$

where $e_{h,l}$ is the upward flux emitted by the land area (h, l), $f(x_h, y_l, x', y', z_i, \omega_j, K_k)$ is the propagation function, z_i, ω_j, K_k are an adequate discretization of the variables z, ω, K and the summations are extended to all land areas around the site inside a distance for which their contributions are non-negligible. We divided the territory in the same land areas covered by pixels of the satellite data. We obtained the propagation function f, expressed as total flux per unit area of the telescope per unit solid angle per unit total upward light emission, with models for the light propagation in the atmosphere based on Garstang models (Garstang 1986, 1989a):

$$f = \int_{u_0}^{\infty} [\beta_{\mathrm{m}}(h) f_{\mathrm{m}}(\varpi) + \beta_{\mathrm{a}}(h) f_{\mathrm{a}}(\varpi)] \times (1 + D_{\mathrm{S}}) i(\psi, s) \xi_1(u)\, \mathrm{d}u, \tag{3}$$

where $\beta_{\mathrm{m}}(h)\, \beta_{\mathrm{a}}(h)$ are, respectively, the scattering cross-sections of molecules and aerosols per unit volume at the altitude h, depending on the distance u along the line of sight of the observer; f_{m} and f_{a} are their normalized angular scattering functions (see Section 3.3), ϖ is the scattering angle, $\xi_1(u)$ is the extinction of the light along its path from the scattering volume to the telescope, $i(\psi, s)$ is the direct illuminance per unit flux produced by each source on each infinitesimal volume of atmosphere along the line of sight and $(1 + D_{\mathrm{S}})$ is a correction factor that takes into account the illuminance due to light already scattered once from molecules and aerosols. It can be evaluated by methods due to Garstang (1984, 1986), neglecting third- and higher-order scattering, which can be significant for optical thicknesses higher than about 0.5. Geometric relations and formulae accounting for Earth curvature have been given and discussed by Garstang (1989a, section 2.2–2.5, equations 4–24). In Garstang 's formulae the molecular scattering cross-section per unit volume is $\beta_{\mathrm{m}} = N_{\mathrm{m}} \sigma_{\mathrm{R}}$.

In the same way as did Garstang (1989a), but differently from Cinzano et al. (2001a), we take into account the elevation both of the source and of the site.

Screening by terrain elevation was accounted for as described in Cinzano et al. (2001a). The illuminance per unit flux was set in equation (3) to

$$i(\psi, s) = I(\psi) \xi_2 / s^2, \tag{4}$$

where there is no screening by Earth curvature or by terrain elevation and $i(\psi, s) = 0$ elsewhere. Here $I(\psi)$ is the normalized emission function giving the relative light flux per unit solid angle emitted by each land area at the zenith distance ψ, s is the distance between the source and the considered infinitesimal volume of atmosphere and

ξ_2 is the extinction along the light path, given by Garstang (1989a). We check each point along the line of sight to determine if the source area is blocked by terrain elevation or not, taking into account the Earth 's curvature, by determining the position of the foot of the vertical of the point considered. Then we computed, for every land area crossed by the line connecting this foot and the source area, the quantity $\cot\psi$ (Cinzano et al. 2001a):

$$\cot\psi = \frac{(A+E) - (h+E)\cos(D/E)}{(h+E)\sin(D/E)}, \tag{5}$$

where A is the elevation of the land area, D is the distance of its centre from the centre of the source area and E is the Earth 's radius. From this we determined the screening elevation h_s:

$$h_s = \frac{A+E}{\cos(D^\star/E) - \max(-\cot\psi)\sin(D^\star/E)} - E, \tag{6}$$

where $D^\star$ is the distance between the source area and the foot of the vertical, and h_s is computed above sea level. The illuminance i in equation (3) is set to zero when the elevation of the point considered is lower than the screening elevation. To speed up the calculation we computed the array only once, which gives the screening elevation for each point along the line of sight, for each azimuth of the line of sight and for each source, and we used it for any computation with different atmospheric parameters. We considered land areas as point sources located in their centres except when $i = h$, $j = k$, in which case we used a four-points approximation (Abramowitz & Stegun 1964). We assumed the elevation given by GTOPO30 to be the same everywhere inside each pixel.

Another array was obtained for the natural sky brightness with the model introduced by Garstang (1989a, section 3). The array $b_{\mathrm{N}i,j,k}$ is the sum of (i) the directly transmitted light b_d that arrives at the observer after extinction along the line of sight (Garstang 1989a, equation 30), (ii) the Rayleigh scattering of light by molecules, b_r (Garstang 1989a, equation 37), and (iii) the light scattered by aerosols, b_a (Garstang 1989a, equation 32):

$$b_{\mathrm{N}i,j,k} = b_{\mathrm{d}i,j,k} + b_{\mathrm{r}i,j,k} + b_{\mathrm{a}i,j,k}. \tag{7}$$

In the computation of the natural sky brightness outside the scattering and absorbing layers of the atmosphere (Garstang 1989a, equation 29), we assumed the brightness of a layer at infinity due mainly to integrated star light, diffused galactic light and zodiacal light, and the brightness of the van Rhijn layer due to airglow emission, to be independent variables.

The array of the total sky brightness is $b_{\mathrm{T}i,j,k} = b_{\mathrm{i,j,k}} + b_{\mathrm{N}i,j,k}$. The sky brightness in the chosen photometric band was expressed as photon radiance (in ph cm^{-2} s^{-1} sr^{-1}) or in magnitudes per arcsec^2 (Garstang 1989a, equations 28 and 39).

We determined the observer 's horizon computing the altitudes below which the line of sight encounters screening by terrain, such as a mountain, and set the total brightness to be zero below them. They are obtained by evaluating the elevation h_T of terrain at distance d along each azimuthal direction and computing the maximum screening altitude angle ϑ:

$$\vartheta = \max\arctan(h_T/d). \tag{8}$$

From the array of the total sky brightness in the V-band, we can obtain a family of other arrays giving the naked-eye star visibility and the telescopic limiting magnitude. The magnitude over the atmosphere of a star at the threshold of visibility to an observer when the brightness of the observed background is b_{obs} in nanolamberts and the stimulus size, i.e. the seeing disc diameter, is θ in arcmins, has been given by Garstang (2000b) based on measurements of Blackwell (1946) and Knoll, Tousey & Hulburt (1946) and on a threshold criterion of 98 per cent probability of detection:

$$m_{\mathrm{star}} = -13.98 - 2.5\log i_1' i_2'/(i_1' + i_2'), \tag{9}$$

with:

$$i_1' = F_1 c_1 \left(1 + k_1 b^{1/2}\right)^2 \left(1 + \alpha_1\theta^2 + y_1 b_{\mathrm{obs}}^{z_1}\theta^2\right), \tag{10}$$

$$i_2' = F_2 c_2 \left(1 + k_2 b^{1/2}\right)^2 \left(1 + \alpha_2\theta^2 + y_2 b_{\mathrm{obs}}^{z_2}\theta^2\right), \tag{11}$$

$$F_1 = F_{\mathrm{a},1} F_{\mathrm{SC},1} F_{\mathrm{cs},1} F_{\mathrm{e},1} F_{\mathrm{s},1}, \tag{12}$$

$$F_2 = F_{\mathrm{a},2} F_{\mathrm{SC},2} F_{\mathrm{cs},2} F_{\mathrm{e},2} F_{\mathrm{s},2}, \tag{13}$$

where i_1' and i_2' are the illuminations produced by the star, related respectively to the thresholds of scotopic and photopic vision, and the fraction is an artefact introduced by Garstang in order to put together smoothly the two components obtaining the best fit with cited measurements. Here F_a takes into account the ratio between pupil areas of the observer and the pupil diameter used by the average of the Knoll, Tousey, Hulburt and Blackwell observers, F_{SC} takes into account the Stiles–Crawford effect, due to the decreasing of the efficiency to detect photons with the distance from the centre of the pupil, producing a non-linearity in the increase of sensibility when the eye pupil increases, F_{cs} allows for the difference in colour between the laboratory sources used in determining the relationships between i and b and the observed star, F_e allows for star light extinction in the terrestrial atmosphere because star magnitudes are given *outside the atmosphere*, F_s allows for the acuity of any particular observer, defined so that $F_s < 1$ implies an eye sensitivity higher than average due possibly to above-average retinal sensitivity, scientific experience or an above-average eye pupil size. Formulae have been given by Schaefer (1990) and Garstang (2000b) and applied by Cinzano et al. (2001a, equations 28–31) to which we refer the reader. The constants c, k, α, y, z in equation (10) are given by Garstang (2000b). The perceived background b_{obs} is related to the total sky brightness under the atmosphere in the V-band given by our hypermaps, converted from photon radiance to nanolamberts (Garstang 2000b):

$$b_{\mathrm{obs}} = b_T/(F_a F_{SC} F_{cb}), \tag{14}$$

where F_{cb} allows for the difference in colour between the laboratory sources and the night sky background, and F_a and F_{SC} have already been described. As a result we obtain the array $m_{i,j,k}$ of the visual limiting magnitude. The array of the telescopic limiting magnitudes can be calculated for the chosen instrumental set-up in a similar way (see the cited authors).

3 INPUT DATA

We summarize here the required input data, which has already been described and discussed by Cinzano et al. (2000, 2001a). We refer the reader to their paper for details. We extended the input data to other continents in the same way.

3.1 Upward light emission data

To compute the illuminance per unit flux i in equation (4) we need the relative intensity $I(x, y, \psi, \chi)$ emitted by every land area in (x, y) at azimuth χ and zenith distance ψ, i.e. the normalized emission function obtained measuring the relative emitted flux per unit solid angle per unit area in the direction ψ and normalizing its integral to unity. If the land areas contain many light installations

randomly distributed in type and orientation, we can assume this function to be axisymmetric, $I(x, y, \psi)$. The corresponding absolute intensity is

$$I'(x, y, \psi) = e(x, y)\, I(x, y, \psi), \tag{15}$$

where $e(x, y)$ is the total upward flux obtained from radiance calibrated data (Cinzano et al. 2001a, equation 35).

We obtained the upward flux $e(x, y)$ on a 30×30 arcsec^2 pixel size grid from the Operational Linescan System (OLS) carried by DMSP satellites after special requests to the US Air Force made by the US Department of Commerce, NOAA National Geophysical Data Centre (NGDC), which serves as the archive for the DMSP and develops night-time lights processing algorithms and products. OLS is an oscillating scan radiometer with low-light visible and thermal infrared (TIR) high-resolution imaging capabilities (Lieske 1981). The OLS Photo Multiplier Tube (PMT) detector has a broad spectral response covering the range for primary emissions from the most widely used lamps for external lighting. The primary reduction steps were (Elvidge et al. 1999; Cinzano et al. 2000, 2001a) as follows.

(i) acquisition of special OLS-PMT data at a number of reduced-gain settings to avoid saturation on major urban centres and, at the same time, to overcome PMT dynamic-range limitation. On-board algorithms that adjust the visible band gain were disabled;

(ii) establishment of a reference grid with finer spatial resolution than the input imagery;

(iii) identification of the cloud free section of each orbit based on OLS-TIR data;

(iv) identification of lights, removal of noise and solar glare, cleaning of defective scan lines;

(v) projection of the lights from cloud-free areas from each orbit into the reference grid;

(vi) calibration to radiance units using preflight calibration of digital numbers for given input telescope illuminance and gain settings in simulated space conditions;

(vii) tallying of the total number of light detections in each grid cell and calculation of the average radiance value;

(viii) filtering images based on frequency of detection to remove ephemeral events;

(ix) transformation into latitude/longitude projection with 30×30 arcsec^2 pixel size;

(x) Lucy–Richardson deconvolution to improve predictions for sites near sources (when possible this should be more properly done before step vii);

(xi) determination of the upward light intensity accounting for the estimated atmospherical extinction in the light path from ground to the satellite, the assumed average spectrum of night-time lighting (Cinzano 2000a, equations 28–30) and the surface of the land areas.

We can obtain $I(x, y, \psi)$ from the radiance measured in a set of individual orbit satellite images where the land area in (x, y) is seen at different angles ψ which are related to the distance D from the satellite nadir (Cinzano et al. 2000, equations 17 and 18). The emitted flux per solid angle per unit area in the direction ψ is obtained from the measured radiance dividing by the extinction coefficient $\xi_3(\psi)$ computed for a curved Earth (Cinzano et al. 2000, equation 19). A study to obtain $I(x, y, \phi)$ in this way for every land area from DMSP-OLS individual orbit data is in progress (Cinzano, Falchi & Elvidge, in preparation). To be simple we assumed here that all land areas have on average the same normalized emission function, given by the parametric representation of Garstang (1986) in equation (15) of Cinzano et al. (2000), which has been tested by studying in a single-orbit satellite image the relation between the upward flux per unit solid angle per inhabitant of a large number of cities and their distance from the satellite nadir (Cinzano et al. 2000) and with many comparisons between model predictions and measurements by Garstang and by Cinzano (2000b). Likely it cannot be applied in areas where effective laws against light pollution are enforced or with unusual lighting habits.

3.2 Elevation data

As input elevation data, we used GTOPO30 – a global digital elevation model by the US Geological Survey 's EROS Data Centre (Gesch, Verdin & Greenlee 1999). This global data set covers the full extent of latitude and longitude with a horizontal grid spacing of 30 arcsec as our composite satellite image. The vertical units represent elevation in metres above mean sea level, which ranges from -407 to 8752 m. We reassigned a value of zero to ocean areas, masked as 'no data' with a value of -9999, and to altitudes below sea level.

3.3 Atmospheric data

In order to evaluate scattering and extinction, we need a set of functions giving, for each triplet of longitude, latitude and elevation (x, y, h), the molecular and aerosol cross scattering coefficients per unit volume of atmosphere $\beta_{\rm m}(x, y, h)$ and $\beta_{\rm a}(x, y, h)$, and the aerosol angular scattering function $f_{\rm a}(\omega, x, y, h)$. The molecular angular scattering function $f_{\rm m}(\omega)$ is known because it is Rayleigh scattering. The atmospheric data needed for reference on a *typical* clean night at the chosen time of year must include information on denser aerosol layers, volcanic dust and the ozone layer.

For simplicity, we applied here the standard atmospheric model already adopted by Garstang (1986, 1989a) and Cinzano et al. (2000, 2001a), neglecting geographical gradients and local particularities. It assumes:

(i) the molecular atmosphere is in hydrostatic equilibrium under the gravitational force, as in Garstang (1986);

(ii) the atmospheric haze aerosol's number density decreases exponentially, as in Garstang (1986);

(iii) a negligible presence of sporadic denser aerosol layers, volcanic dust and ozone layer (as studied by Garstang 1991a,c));

(iv) the normalized angular scattering function for atmospheric haze aerosols given in Garstang (1991a);

(v) the aerosol content given by an atmospheric clarity parameter that measures the relative importance of aerosol and molecules for the scattering of light.

The Garstang atmospheric clarity parameter K measures the relative importance of aerosols and molecules for scattering light in the V-band at ground level (Garstang 1986):

$$K = \frac{\beta_{{\rm a},H}}{\beta_{{\rm m},0} 11.11 {\rm e}^{-cH}}, \tag{16}$$

where H is the altitude of ground level above sea level and c is the inverse scale-height of molecules. It assumes that there is only one ground level where all the polluting sources lie. To be more self-consistent when there are many cities at different elevations above sea level, we introduced an atmospheric clarity parameter K' defined at sea level:

$$K' = \frac{\beta_{{\rm a},0}}{\beta_{{\rm m},0} 11.11}, \tag{17}$$

such that, at the ground level of each city, $K = K' e^{(c-a)H}$, where a is the inverse scale-height of aerosols. We can associate the atmospheric clarity K with vertical extinction (e.g. Garstang 1991a, equation 6) and with other observable quantities like the horizontal visibility (Garstang 1989a, equation 38), the optical thickness τ (Garstang 1986, equation 22) and the Linke turbidity factor for total solar radiation (Garstang 1988). Extinction along light paths for this atmospheric model was given by Garstang (1989a, equations 18–22).

3.4 Natural night sky brightness data

The brightness $b_{S\,i,j}$, due to integrated star light, diffused galactic light and zodiacal light, depends on the observed area of the sky and on the time. This dependence on the position in the sky is important when sky maps are made to quantify the visibility of astronomical phenomena, otherwise we can assume $b_{S\,i,j}$ constant and given by its average value at the site considered. The brightness of the Van Rhijn layer, b_{VR}, depends on some factors like the geographical position, the solar activity during the previous daytime, and the time after twilight. We referred our predictions to some hours after twilight, when the night brightness decays at a constant value (Walker 1988, but see also Patat 2003a), and to minimum solar activity. If requested, the solar activity can be roughly accounted as in Cinzano et al. (2001a) or, more accurately, based on the correlation with the 10.7-cm solar radio flux (Walker 1988; Krisciunas 1999). The dependence of b_{VR} on geographical position suggests studying the natural sky brightness in the nearest unpolluted site, which can be located in the world atlas of artificial sky brightness (Cinzano et al. 2001b), in order to obtain $b_{S\,i,j}$ and b_{VR}. When only one or few measurements were available we assumed as did Garstang (1989a) that $b_{S\,i,j} = 0.4\ b_0$ and $b_{VR} = 0.6\ b_0$ and determined b_0.

4 DISENTANGLING INDIVIDUAL CONTRIBUTIONS

We can make some analysis of the contributions from each 30×30 arcsec^2 land area that enters into the summations of equation (2). First we can make hypermaps of sky brightness produced by individual land areas and compare them. Moreover, given an array cell of index (i, j, k) we can obtain a geographic map showing the contribution $b_{i,j,k}(x_h, y_l)$ produced by each land area in (x_h, y_l), searching for the main polluting sources and calculating some statistics about their geographic distribution:

$$b_{i,j,k}(x_h, y_l) = e_{h,l} f(x_h, y_l, x', y', z_i, \omega_j, K_k). \quad (18)$$

We can obtain hypermaps of sky brightness produced by each city or territory identifying pixels belonging to each city or territory of a given list and summing their contributions:

$$b_{i,j,k}(n) = \sum_{\substack{h,l \\ n\text{th city}}} e_{h,l} f(x_h, y_l, x', y', z_i, \omega_j, K_k). \quad (19)$$

Their comparison is helpful, for example, to understand if larger contributions come from a few main cities or from many small towns, even in relation to atmospheric conditions. The fraction of sky brightness produced in a given array cell (i, j, k) by the sources inside a circular area of radius d can be obtained by summing all contributions of land areas inside the distance d from the site and dividing by the sum of all contributions:

$$b^\star(d) = \frac{1}{b_{i,j,k}} \sum_{\substack{h,l \\ (x_h-x')^2+ \\ (y_l-y')^2 \leqslant d^2}} e_{h,l} f(x_h, y_l, x', y', z_i, \omega_j, K_k). \quad (20)$$

This is useful, for example, to evaluate the effectiveness of protection areas (Cinzano 2000c).

5 APPLICATION

The software package LPSKYMAP, written in FORTRAN-77, calculates the artificial night sky brightness, the total night sky brightness and the star visibility (limiting magnitude) over the entire sky at any site in the world. The availability of OLS-DMSP fixed gain data on a yearly or sub-yearly time-scale will allow a fine time resolution.

Results are arrays of the artificial night sky brightness, the total night sky brightness, the visual limiting magnitude and the loss of visual limiting magnitude. Each hypermap array is composed of a series of 19×37 pixel images in cartesian coordinates, one for each aerosol content K, spline interpolated over 91×181 pixels in cartesian coordinates or projected in 721×721 pixels in polar coordinates. Images go from 0 to 360 degrees in azimuth, starting from East (in order to avoid placing the meridian at the borders) toward South, and from horizon to zenith in altitude. They are saved in 16-bit standard FITS format with FITSIO FORTRAN-77 routines developed by HEASARC at the NASA/GSFC. ASCII data tables are also provided. The night sky brightness in the chosen photometric band is given as photon radiance in ph s^{-2} m^{-2} sr^{-1} or as astronomical brightness in mag arcsec^{-2}. Brightness in the V-band can also be expressed as luminance in μcd m^{-2}, using Garstang 's conversion (Garstang 2002; Cinzano 2004). From the hypermap arrays we can obtain the following.

(i) sections perpendicular to the K-axis: $b(z, \omega, K = K_0)$. They are the maps of the sky brightness or limiting magnitude for a given aerosol content and they correspond to each individual image of the series;

(ii) secants parallel to the K-axis: $b(z = z_0, \omega = \omega_0, K)$. They provide the brightness or the limiting magnitude in a given point of the sky as the aerosol content changes;

(iii) secants perpendicular to the K- and ω-axis: $b(z, \omega = \omega_0, K = K_0)$. They give the brightness or the limiting magnitude along an almucantar, e.g. the meridian, for a given aerosol content.

The arrays computation steps are as follows.

(i) an input file is prepared with the geographical position and elevation of the site, the names of the input DEM and lights frames and the position of their upper left corner;

(ii) the array, i.e. the series of images, of the artificial night sky brightness is computed with the program LPSKYMAP for a given range and step of the aerosol content, accounting for the Earth 's curvature and elevation but not for screening. The radius of the contributing area can be 250 km for sites in urbanized areas or 350 km for dark sites;

(iii) subimages with DEM and light data have been cropped from the original large-scale frames with the program MAKEFRAC. We use FITS or RAW images 701×701 pixels in size to limit the requirements of RAM memory during screening computation. They are checked for relative mismatches that can be corrected with the program MAKESHIFT;

(iv) the screening angles for each direction of observation and for each area inside a given radius from the site are computed with the program MAKESCREEN. We limited the radius to 200 km to avoid too long a computation time. The program writes the screening data of each site in 106 files for a total size of 20 GB uncompressed. It also calculates the horizon line as seen by the site. DEM pixels very near to the site are divided into 11×11 sub-pixels evaluated separately;

(v) an array containing the screened brightness is computed with the program LPSKYSCREEN when there are reasons to believe that screening is not negligible;

(vi) the images of the screened brightness array are subtracted from the corresponding images of the sky brightness array, after properly re-scaling, in order to obtain the array of the night sky brightness corrected for mountain screening;

(vii) the array is calibrated with the program LPSKYCAL based on pre-flight calibration to 1996–1997, or on Cinzano et al. (2001b) calibration to 1998–1999 made with Earth-based measurements, or on observations taken at the same site. The measurements of Cinzano et al. (2001a) fitted predictions based on the pre-flight calibration with $\sigma \leqslant 0.35$ mag arcsec^{-2} and a shift $\Delta m = -0.28$ mag arcsec^{-2}, probably mainly due to the growth of light pollution in the period between the observations and the satellite data acquisitions. The program adds the natural sky brightness, producing a series of calibrated maps of the total night sky brightness, interpolated or not, and the limiting magnitude. It also adds the horizon line. It does not account for the refraction of light by the atmosphere, which could increase the brightness near the horizon towards very far cities;

(viii) maps in polar coordinates are obtained with the program LPSKYPOLAR. East is up, North at right;

(ix) maps are analysed with FTOOLS, developed by HEASARC at the NASA/GSFC;

(x) comparison with observations is made with the program LPSKYCOMPARE. Measurements should be 'under the atmosphere'. Statistical analysis is made with the software MATHEMATICA of Wolfram Research.

A number of utility programs complete the package. The computation time depends on the geographical behaviour of the site, like the quantity of dark pixels, the quantity of non-zero elevation pixels, etc. As an example, the computation of one element of the array (i.e. a single map for a given atmospheric content) for Sunrise Rock on a workstation with Xeon processor running at 1700 MHz required about 35 h for LPSKYMAP, 10 h for MAKESCREEN and 6 h for LPSKYSCREEN. However, the computation with LPSKYMAP for the site in Padua required 80 h, even if restricted inside a radius of 250 km, whereas the same computation for Serra La Nave required only 18 h.

6 RESULTS

In this section we present a sample of results that can be obtained with our method and some comparisons with available measurements. Specific studies are reserved for forthcoming papers.

The NGDC 's request for the low- and medium-gain DMSP-OLS data used in this work was granted by the US Air Force for the darkest nights of lunar cycles in 1996 March and 1997 January–February. More recent data sets taken in the period 1999–2003 are already at our disposal, but they are still under reduction and, before we are able to use them, we need to solve a number of problems in the analysis process (Cinzano, Falchi & Elvidge, in preparation). Preflight calibration of upward flux refers to 1996–1997, to the average lighting spectra of Cinzano et al. (2000) and to an average vertical extinction in the V-band at imaging time assumed to be $\Delta m = 0.33$ mag. All results are computed for minimum solar activity and refer to some hours after twilight. We tuned the parameter b_0 to fit the zenith natural sky brightness for a clean atmosphere as measured by Cinzano et al. (2001a) at Isola del Giglio, Italy, $V = 21.74 \pm 0.06$ mag arcsec^{-2} in the V-band for average solar activity and 200-m altitude above sea level. It agrees well with the average natural night sky brightness of 21.6 mag arcsec^{-2} measured by Patat (2003a) at ESO-Paranal. In fact, the sky become darker going to lower elevation above sea level owing to larger extinction, even if this phenomenon is limited by the increase of the light scattered from aerosols and molecules along the line of sight (Garstang 1989a). Patat (2003a) reported a large contribution from zodiacal light, about 0.18 mag arcsec^{-2}, which justifies the fact that he finds the sky slightly more luminous than expected. The algorithm of Patat (2003b) applied to VLT images excludes almost completely the stellar component whereas Cinzano et al. (2001a) excluded only stars fainter than 18th magnitude, but the expected difference is only $\approx$0.03 mag arcsec^{-2}. The 'visual' natural night sky brightness should be obtained from the measured one adding the average stellar background produced by stars with magnitude $\geqslant 7$ missed by the instrument or the analysis (Cinzano & Falchi 2004). This contribution is about -0.26 mag arcsec^{-2} when stars down to magnitude 24 are missed. In our brightness predictions we did not correct the natural night sky brightness to the visual value.

Fig. 2 shows the night sky brightness at Sunrise Rock, a site located in Mojave National Preserve, California, USA (longitude 115°33′6.4″W, latitude 35°18′57.7″N) at 1534 m above sea level. This site is mainly polluted by the lights of Las Vegas, about 100 km away. The azimuth goes from 0 to 360 degrees, starting from East towards South. Figures with full colour scale are available in the online version of the journal on *Synergy*, whereas in the paper version we adopted a cyclic greyscale which enhances some contours of the brightness distribution. Fig. 3 shows the night sky brightness screened by mountains, which amounts to a few hundredths of a magnitude. Fig. 4 shows a comparison between predictions for atmospheric clarities $K' = 0.5$ (squares) or $K' = 3$ (crosses) and the V-band measurements taken on 2003 May 8 at 05.34–06.00

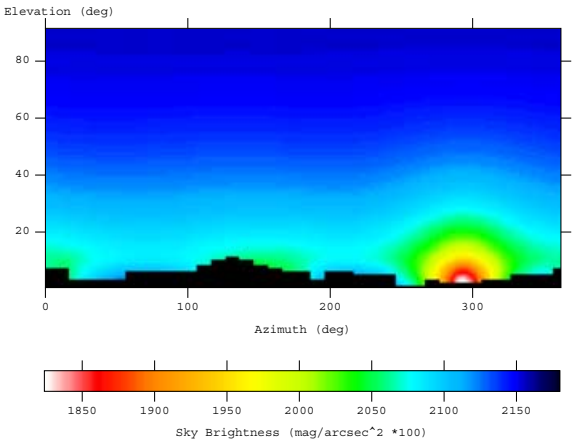

Figure 2. Night sky brightness at Sunrise Rock, USA for atmospheric clarity $K' = 0.5$.

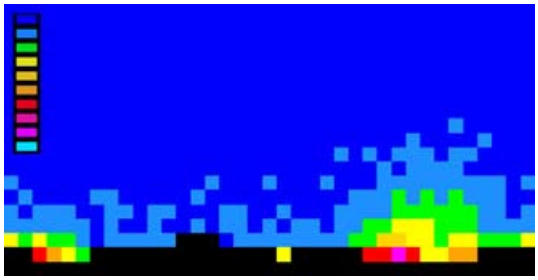

Figure 3. Brightness screened by mountains at Sunrise Rock, USA for atmospheric clarity $K' = 0.5$. Each level from blue to violet is 0.01 mag arcsec^{-2}.

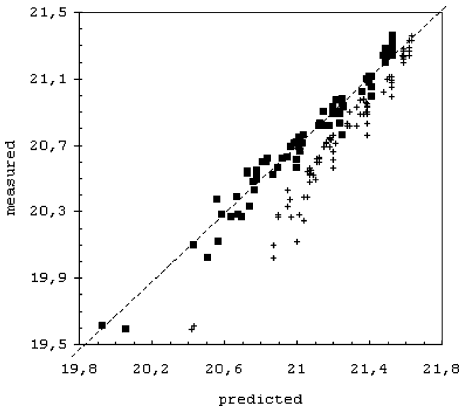

Figure 4. Comparison between predictions and V-band measurements at Sunrise Rock for atmospheric clarities $K' = 0.5$ (squares) and $K' = 3$ (crosses). Units are mag arcsec^{-2}.

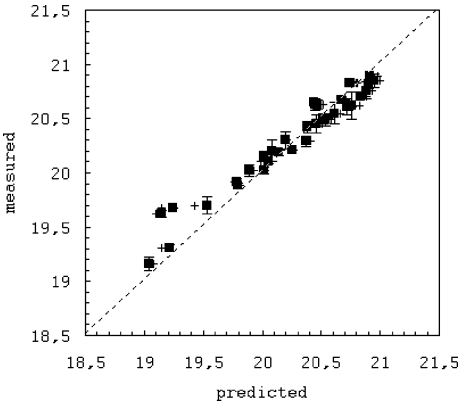

Figure 6. Comparison between predictions and V-band measurements at Serra la Nave Observatory for atmospheric clarities $K' = 1$ (squares) and $K' = 2$ (crosses). Units are mag arcsec^{-2}.

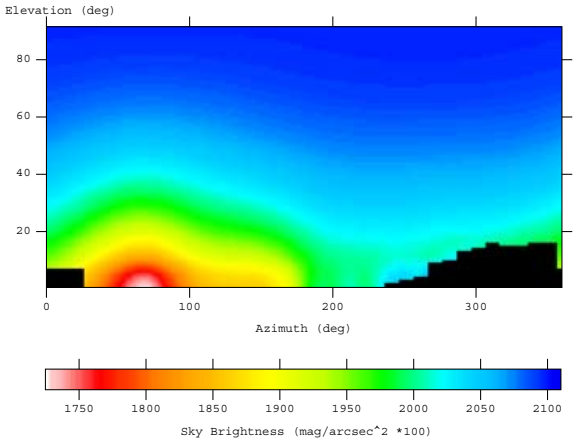

Figure 5. Night sky brightness at Serra la Nave Observatory, Italy for atmospheric clarity $K' = 1$.

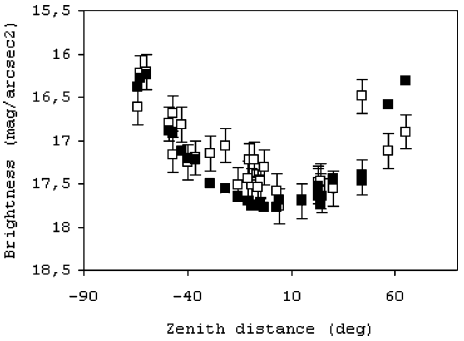

Figure 7. Brightness–zenith distance relation measured at G. Ruggeri Observatory, Italy (open symbols) and predictions for the same viewing directions (filled symbols) for atmospheric clarity $K' = 3$ versus the zenith distance. Positive elevations collect measurements with zenith distances less than $\pm 90^\circ$ from the direction of the city centre.

UT (Duriscoe, Moore & Luginbuhl 2004) with vertical extinction $k_V = 0.18$ mag. The agreement is excellent after a uniform scaling of about -0.3 mag arcsec^{-2}. It suggests an increase of light pollution from 1997 to 2003 of $\approx$5 per cent per year, slightly less than the average yearly growth of $\approx$6 per cent estimated by Cinzano (2003). A comparison with a data set taken on 2003 September 22 at 06.27–06.58 UT with $k_V = 0.26$ mag gives similar results.

Fig. 5 shows the night sky brightness at Serra la Nave Observatory (longitude 14°58′24″E, latitude 37°41′30″N) at 1734 m above sea level on the Mt Etna volcano, Italy. This site is situated at few kilometres from a densely populated area with $\sim 1.8 \times 10^6$ inhabitants, which includes the cities of Catania (23 km) and Messina (75 km). Fig. 6 shows a comparison between predictions for atmospheric clarities $K' = 1$ (squares) and $K' = 2$ (crosses) with the V-band measurements taken on 1998 February 22–23 at 18.00–20.00 UT with vertical extinction $k_V = 0.26$ mag (Catanzaro & Catalano 2000; see fig. 2). The agreement is good. The fit is slightly better for the model with $K' = 1$, corresponding to a vertical extinction of $k_V = 0.17$ mag, which is smaller than the measured one. However the vertical extinction at this site could be locally determined by the volcanic dust (Catanzaro, private communication) whereas K' depends on the average aerosol content of the entire area with 250-km radius, so they do not need to match.

The effect of an increase of the aerosol content depends on the distribution of sources around the site. In general it decreases the zenith brightness when the distance of the main sources is larger than a few kilometres, decreases the brightness at low elevation in the direction of far sources, and increases the brightness at very-low elevation in the direction of sources at small or average distance. This could explain the different dependence of sky brightness on aerosol content at these two sites.

Fig. 7 shows the night sky brightness versus the zenith distance at G. Ruggeri Observatory, Padova, Italy (longitude 11°53′20″E, latitude 45°25′ 10″N). This site is located inside a city of 8×10^5 inhabitants in a plain with more than 4×10^6 inhabitants. Positive zenith distances collect measurements with azimuth inside $\pm 90^\circ$ from the direction of the city centre. Open symbols are V-band measurements taken on 1998 March 26 at 20.00–23.30 UT, with $k_V = 0.48$ mag (Favero et al. 2000). Filled symbols are predictions in the same directions for atmospheric clarity $K' = 3$, corresponding to $k_V = 0.65$ mag. For smaller values of K' the brightness is underestimated by a constant value. This is probably due to the fact that our model cannot accurately account for the scattered light coming from lighting installations inside a few hundreds of metres from the site because pixel sizes are of the order of 1 km. We used for this prediction the calibration made for 1998–1999 by Cinzano et al. 2001a. For an atmospheric clarity $K \geqslant 2.2$, i.e. for an optical depth $\tau \geqslant 0.5$, the double scattering approximation could be not fully adequate (Garstang 1989a; Cinzano et al. 2000). Fig. 8 shows the contribution to the artificial night sky brightness produced in the

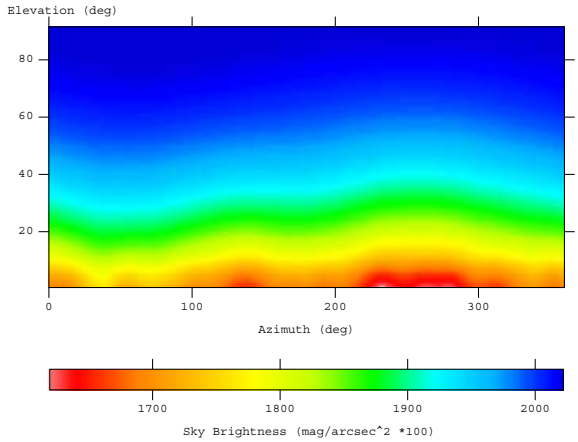

Figure 8. Contribution to the artificial night sky brightness at Padua from sources outside Padua for atmospheric clarity $K' = 1$.

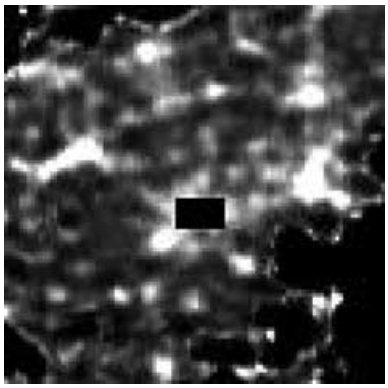

Figure 9. Distribution of lights in the plain surrounding Padua from OLS-DMSP satellite data. Dark section is the neglected area in the prediction of Fig. 8. The region shown is 50-arcmin square in geographic latitude/longitude projection (approximately 65 × 93 km).

same site from the sources outside Padua for atmospheric clarity $K = 1.9$ ($k_V = 0.48$ mag). The area neglected in the prediction is shown in Fig. 9 together with the distribution of lights in the Padana Plain surrounding Padua from OLS-DMSP satellite data.

Fig. 10 shows in polar coordinates the total night sky brightness in the V-band at Mt Graham Observatory, USA (longitude 109°53′31″W, latitude 32°42′5″N, 3191-m above sea level) for atmospheric clarity $K' = 0.5$. It can be compared with the image available at the web address http://mgpc3.as.arizona.edu/images/Night%20Sky%20large.jpg or with fig. 8 of Garstang (1989a), which shows only the artificial brightness.

Fig. 11 shows the naked-eye limiting magnitude at Sunrise Rock. Limiting magnitude is computed for observers of average experience and capability $F_s = 1$, aged 40 yr, 98 per cent detection probability (faintest star that the observer sees *surely* and not the faintest *suspected* star) and star colour index $B–V = 0.7$ mag. Experienced amateur astronomers are more trained in naked-eye observation than inexperienced people and can consider a star to have been detected at a much smaller detection probability, so that their limiting magnitude can be more than one magnitude larger (Schaefer 1990). See the discussion in Cinzano et al. (2001a).

We checked the effects of the mountain screening trying to reproduce the umbrae on the sky modelled by Schaefer (1988) and due

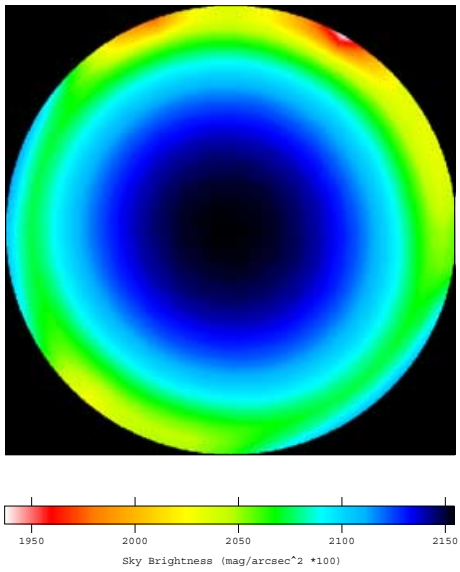

Figure 10. Night sky brightness in the V-band at Mt Graham Observatory, USA in polar coordinates for atmospheric clarity $K' = 0.5$. The figure is plotted with East at bottom, North at left.

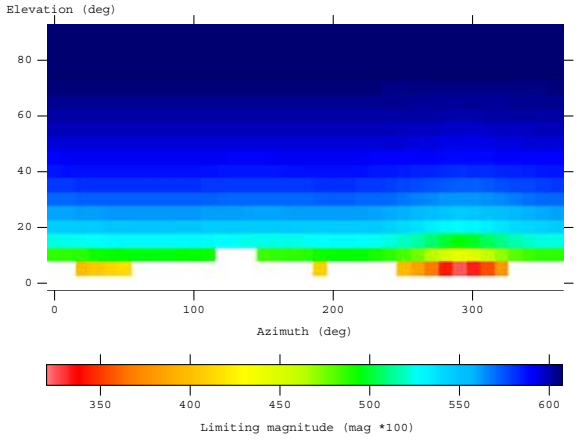

Figure 11. Naked eye limiting magnitude at Sunrise Rock, USA for atmospheric clarity $K' = 0.5$ and 98 per cent detection probability.

to the screening produced by Mauna Kea on the light of the rising sun backscattered to the observer. Fig. 12 shows the analogue of Schaefer's umbrae produced by a source of light pollution instead of the Sun. A city screened by a large conic mountain (left) projects an umbra over the horizon (right). When the mountain is off-set in respect to the observer–source line, a non-symmetric penumbra appears. Here the penumbra is at higher altitudes than in the Wynn–Williams photo (Schaefer 1988, fig. 1) because the observer is at lower elevation. Further examples of umbrae and baffles are shown by Cinzano & Elvidge (2003a, figs 1 and 3; 2003b).

7 CONCLUSIONS

We extended the seminal works of Garstang by applying his models to upward flux data from DMSP satellites and to GTOPO30 digital elevation models, and by accounting for mountain screening. The method presented allows one to monitor the artificial sky brightness

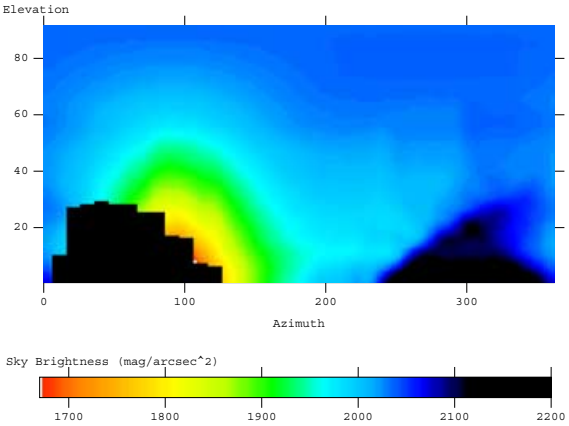

Figure 12. A city screened by a large mountain (left), off-set with respect to the observer–source line, projects an asymmetric Schaefer umbra on the sky (right). Brightness scale is arbitrary.

and visual or telescopic limiting magnitudes at astronomical sites or in any other site in the world.

This study provides fundamental information for evaluating observing sites suitable for astronomical observations, to quantify sky glow, to recognize endangered parts of the sky hemisphere when measurements are not readily available or easily feasible, and to quantify the ability of the resident population to perceive the Universe they live in. The method enables one to study the relationship of night sky brightness to aerosol content and to evaluate its changes with time. The method also allows one to analyse the adverse impacts on a site from the surrounding territories, making it possible to disentangle individual contributions in order to recognize those that are producing the stronger impact and hence to undertake actions to limit light pollution (the use of fully shielded fixtures, limitation of the downward flux wasted outside the lighted surface, use of lamps with reduced scotopic emission, flux reduction whenever possible, no lighting where not necessary, restraining of lighting growth rates or lighting density, etc.). We also present some tests of the method. The effects of light pollution on the night sky are easily evident in the maps in the text.

Important refinements need to be made in the future years: (i) it may be possible to derive the angular distribution of light emissions from major sources of night-time lighting from OLS or future satellite data (Cinzano, Falchi, Elvidge, in preparation). This will improve the accuracy of the modelling, in particular where laws against light pollution are enforced; (ii) a global Atlas of the growth rates of light pollution and zenith night sky brightness from satellite data (Cinzano, Falchi, Elvidge, in preparation) will make it possible to predict the evolution of the night sky situation at sites; (iii) a worldwide atmospheric data set giving the atmospheric conditions in any land area for the same nights of satellite measurements or for a typical local clear night will allow the replacement of the standard atmosphere with the true atmosphere or the typical local atmosphere; (iv) the availability of spectra of the light emission of each land area from satellites will allow a more precise conversion of OLS data to astronomical photometrical bands and an accurate modelling of the colours of the night sky; (v) a large number of accurate measurements of night sky brightness and visual limiting magnitude including the evaluation of the atmospheric content, from the vertical extinction for example, will allow the predictions to be better constrained, which in turn will allow improvements in the modelling technique. The International Dark-Sky Association, the organization which takes care of the battle against light pollution and the protection of the night sky, is making a large worldwide effort to collect accurate measurements of both night sky brightness and stellar extinction (e.g. Cinzano & Falchi 2004). They constitute a fundamental component of the monitoring of the night sky situation in the world.

ACKNOWLEDGMENTS

We are indebted to Roy Garstang of JILA-University of Colorado for his friendly kindness in reading this paper, for his helpful suggestions and for interesting discussions. We acknowledge the EROS Data Centre, Sioux Falls, USA for kindly providing us their GTOPO30 digital elevation model and the National Park Service Night Sky Team, Death Valley, USA, together with the authors Dan Duriscoe, Chad Moore and Christian Luginbuhl, for kindly providing us with some of their night sky brightness data. This work has been supported by Italian Space Agency contract I/R/160/02. The application to Padua is part of a research project supported by the University of Padua CPDG023488.

REFERENCES

Abramowitz M., Stegun I. A., 1964, Handbook of Mathematical Functions. NBS, Washington
Blackwell H. R., 1946, J. Opt. Soc. Am., 36, 624
Catanzaro G., Catalano F. A., 2000, in Cinzano P., ed., Measuring and modelling light pollution. Mem. Soc. Astron. Ital., 71, 211
Cinzano P., 1994, Int. Rep. No. 11, References on Light Pollution and Related Fields, Part D. Dep. Astron., University of Padova, http://dipastro.pd.astro.it/cinzano/refer/node8.html
Cinzano P., ed., 2000a, Measuring and modelling light pollution. Mem. Soc. Astron. Ital., 71
Cinzano P., 2000b, in Cinzano P., ed., Measuring and modelling light pollution. Mem. Soc. Astron. Ital., 71, 113
Cinzano P., 2000c, in Cinzano P., ed., Measuring and modelling light pollution. Mem. Soc. Astron. Ital., 71, 93
Cinzano P., ed., 2002, Proc. Light pollution and the protection of the night environment. ISTIL, Thiene, http://dipastro.pd.astro.it/cinzano/
Cinzano P., 2003, in Schwarz H. E., ed., Light Pollution: The Global View. Kluwer, Dordrecht, p. 39
Cinzano P., 2004, preprint
Cinzano P., Elvidge C. D., 2003a, in Schwarz H. E., ed., Light Pollution: the Global View. Kluwer, Dordrecht, p. 29
Cinzano P., Elvidge C. D., 2003b, in Corsini E. M., ed., LV Nat. Meeting Soc. Astron. Ital. Mem. Soc. Astron. Ital., 74, 456
Cinzano P., Falchi F., 2004, IAPPP Comm., 88, 54, in press, http://dipastro.pd.astro.it/cinzano/misure/sbeam2.html
Cinzano P., Falchi F., Elvidge C. D., Baugh K. E., 2000, MNRAS, 318, 641
Cinzano P., Falchi F., Elvidge C. D., 2001a, MNRAS, 323, 34
Cinzano P., Falchi F., Elvidge C. D., 2001b, MNRAS, 328, 689
Cohen R. J., Sullivan W. T., eds, 2001, Proc. IAU Symp., Vol. 196, Preserving the Astronomical Sky. Astron. Soc. Pac., San Francisco
Crawford D. L., ed., 1991, ASP Conf. Ser., Vol. 17, Proc. IAU Coll., Vol. 112, Light Pollution, Radio Interference and Space Debris. Astron. Soc. Pac., San Francisco
Duriscoe D. M., Moore C., Luginbuhl C. B., 2004, Measuring sky quality with a wide angle CCD camera, presented at International Dark Sky Association Annual Meeting, March 12, 2004, Tucson (to be requested to authors)
Elvidge C. D., Baugh K. E., Kihn E. A., Kroehl H. W., Davis E. R., 1997a, Photogram. Eng. Remote Sens., 63, 727
Elvidge C. D., Baugh K. E., Kihn E. A., Kroehl H. W., Davis E. R., Davis, C., 1997b, Int. J. Remote Sens., 18, 1373
Elvidge C. D., Baugh K. E., Hobson V. H., Kihn E. A., Kroehl H. W., Davis E. R., Cocero D., 1997c, Global Change Biol., 3, 387

Elvidge C. D., Baugh K. E., Dietz J. B., Bland T., Sutton P. C., Kroehl H. W., 1999, Remote Sens. Environ., 68, 77
Elvidge C. D., Imhoff M. L., Baugh K. E., Hobson V. R., Nelson I., Safran J., Dietz J. B., Tuttle B. T., 2001, J. Photogram. Remote Sens., 56, 81
Elvidge C. D., Hobson V. R., Nelson I. L., Safran J. M., Tuttle B. T., Dietz J. B., Baugh K. E., 2003a, in Mesev V., ed., Remotely Sensed Cities. Taylor & Francis, London, p. 281
Elvidge C. D., Safran J. M., Nelson I. L., Tuttle B. T., Hobson V. R., Baugh K. E., Dietz, J. B., 2003b, in Lunetta R. S., Lyon J. G., eds, Remote Sensing and GIS Accuracy Assessment. CRC Press, Boca Raton, in press
Erren T. C., Piekarski C., eds, 2002, Light, endocrine systems and cancer. Neuroendocrinology Letters Suppl. 2, Vol. 23
Falchi F., 1998, Tesi di Laurea, Univ. Milan
Falchi F., Cinzano P., 2000, in Cinzano P., ed., Measuring and modelling light pollution. Mem. Soc. Astron. Ital., 71, 139
Favero G., Federici A., Blanco A. R., Stagni R., 2000, in Cinzano P., ed., Measuring and modelling light pollution. Mem. Soc. Astron. Ital., 71, 223
Gallo K. P., Elvidge C. D., Yang L., Reed B. C., 2003, Int. J. Remote Sens., 25, 2003
Garstang R. H., 1984, Observatory, 104, 196
Garstang R. H., 1986, PASP, 98, 364
Garstang R. H., 1987, in Millis R. L., Franz O. G., Ables H. D., Dahn C. C., eds, Identification, optimization and protection of optical observatory sites. Lowell Obs., Flagstaff, p. 199
Garstang R. H., 1988, Observatory, 108, 159
Garstang R. H., 1989a, PASP, 101, 306
Garstang R. H., 1989b, ARA&A, 27, 19
Garstang R. H., 1991a, PASP, 103, 1109
Garstang R. H., 1991b, in Crawford D. L., ed., ASP Conf. Ser., Vol. 17, Proc. IAU Coll., Vol. 112, Light Pollution, Radio Interference and Space Debris. Astron. Soc. Pac., San Francisco, p. 56
Garstang R. H., 1991c, Observatory, 111, 239
Garstang R. H., 1992, BAAS, 24, 740
Garstang R. H., 1993, BAAS, 25, 1306
Garstang R. H., 2000a, in Cinzano P., ed., Measuring and modelling light pollution. Mem. Soc. Astron. Ital., 71, 71
Garstang R. H., 2000b, in Cinzano P., ed., Measuring and modelling light pollution. Mem. Soc. Astron. Ital., 71, 83
Garstang R. H., 2002, Photometric conversion formulae, report presented to CIE Technical Committee 4 (to be requested to authors)
Gesch D. B., Verdin K. L., Greenlee S. K., 1999, EOS Trans. Am. Geophys. Union, 80, 6, 69
Henderson M., Yeh E. T., Gong P., Elvidge C. D., Baugh K., 2003, Int. J. Remote Sens., 24, 595
Isobe S., Hamamura S., 2000, in Cinzano P., ed., Measuring and modelling light pollution. Mem. Soc. Astron. Ital., 71, 131
Isobe S., Hirayama T., eds, 1998, ASP Conf. Ser., Vol. 139, Proc. IAU Joint Discussion 5, Preserving the Astronomical Windows. Astron. Soc. Pac., San Francisco
Knoll H. A., Tousey R., Hulburt E. O., 1946, J. Opt. Soc. Am., 36, 480
Kovalewski J., ed., 1992, NATO Pilot Study 189, The Protection of Astronomical and Geophysical Sites. Editions Frontières, Paris
Krisciunas K., 1997, PASP, 109, 1181
Lieske R. W., 1981, Proc. Int. Telemetry Conf., 17, 1013
Luginbuhl C. B., 2001, in Cohen R. J., Sullivan, W. T., eds, Proc. IAU Symp., Vol. 196, Preserving the Astronomical Sky. Astron. Soc. Pac., San Francisco, p. 103
McNally D., ed., 1994, Proc. IAU–ICSU–UNESCO meeting, The Vanishing Universe. Adverse environmental impacts on astronomy. Cambridge Univ. Press, Cambridge
Osman A. I. I., Isobe S., Nawar S., Morcos A. B., 2001, in Cohen R. J., Sullivan W. T., eds, Proc. IAU Symp., Vol. 196, Preserving the Astronomical Sky. Astron. Soc. Pac., San Francisco, p. 107
Patat F., 2003a, A&A, 400, 1183
Patat F., 2003b, A&A, 401, 797
Rich C., Longcore T., eds, 2002, Symp. abstracts, Ecological Consequences of Artificial Night Lighting, http://www.urbanwildlands.org/ECANLProgram.pdf (see also http://www.urbanwildlands.org/conference.html)
Schaefer B. E., 1988, Sky &Telescope, 4, 416
Schaefer B. E., 1990, PASP, 102, 212
Schwarz H. E., ed., 2003, Light Pollution: the Global View. Kluwer, Dordrecht
Sullivan W. T., 1989, Int. J. Remote Sens., 10, 1
Sullivan W. T., 1991, in Crawford D. L., ed., ASP Conf. Ser., Vol. 17, Proc. IAU Coll., Vol. 112, Light Pollution, Radio Interference and Space Debris. Astron. Soc. Pac., San Francisco, p. 11
Walker M. F., 1988, PASP, 100, 496

This paper has been typeset from a TEX/LATEX file prepared by the author.